Hydrogels for Local and Sustained Delivery of Bacteriophages to Treat Multidrug-Resistant Wound Infections

Yung-Hao Lin[1*], Tejas Dharmaraj[2*], Qingquan Chen[2*], Arne Echterhof[2], Robert Manasherob[3], Lucy Jia Zheng[4], Cas de Leeuw[5], Nana Ansuah Peterson[2], Whitney Stannard[2], Zhiwei Li[2], Maryam Hajfathalian[2], Aviv Hargil[2], Hunter A. Martinez[2], Tony Hong Wei Chang[2], Francis B. Blankenberg[6], Derek Amanatullah[3], Ovijit Chaudhuri[7†] and Paul Bollyky[2†]

[*]Authors contributed equally
[1]Department of Chemical Engineering, Stanford University, Stanford, CA, USA
[2]Division of Infectious Diseases and Geographic Medicine, Department of Medicine, Stanford University School of Medicine, Stanford, CA, USA
[3]Department of Orthopaedic Surgery, Stanford Hospital and Clinics, Redwood City, CA, USA
[4]Department of Material Science and Engineering, Stanford University, Stanford, CA, USA
[5]Institute for Molecules and Materials, Radboud University, Nijmegen, Netherlands
[6]Division of Pediatric Radiology and Nuclear Medicine, Department of Radiology, Lucile Packard Children's Hospital, Stanford, CA, USA
[7]Department of Mechanical Engineering, Stanford University, Stanford, CA, USA

[†]Address correspondence to pbollyky@stanford.edu and chaudhuri@stanford.edu

Abstract
Bacteriophages (phages), viruses that specifically target and kill bacteria, represent a promising strategy to combat multidrug-resistant (MDR) pathogens such as *Pseudomonas aeruginosa* (*Pa*). However, delivering sufficient concentrations of active phages directly to the infection site remains challenging, with current methods having variable success. Here we present “HydroPhage”, an innovative hydrogel system for the sustained release of high-titer phages to effectively treat infections caused by MDR pathogens. Our injectable hydrogels, featuring dual-crosslinking of hyaluronic acid and PEG-based hydrogels through static covalent thioether bonds and dynamic covalent hemithioacetal crosslinks (DCC), encapsulate phages at concentration up to 10^{11} PFU/mL, and achieves controlled release of 10^9 PFU daily over a week, surpassing levels of current clinical dosages, with more than 60% total phage recovery. In a preclinical mouse model of extended wound infection, compared to intravenous treatment, we demonstrate enhanced bacterial clearance by localized, high-dose, and repeated phage dosing despite the emergence of bacterial resistance to phages. This work advances the development of clinically practical wound dressings tailored for resistant infections.

Introduction

Pseudomonas aeruginosa (Pa) is a major human pathogen, responsible for extensive mortality (1), and billions of dollars in health care costs (2,3). Managing *Pa* infections presents a significant challenge due to its resistance to numerous antibiotics (4) including antibiotics of last resort (5–8) . Multidrug-resistant (MDR) *Pa* is recognized as a serious threat by the Centers for Disease Control and Prevention (CDC) and the World Health Organization (WHO), but there are few antibiotics in the clinical pipeline (9,10). Much of the morbidity and economic impact of *Pa* is associated with chronic wound infections. *Pa* is implicated in 35-50% of all chronic wounds (11–14) , particularly diabetic ulcers (15). Commonly, patients with chronic infected wounds receive weekly treatment, including wound debridement, topical antimicrobials, and dressing changes, as part of the standard of care. However, despite the current treatment regimen, *Pa* infections still contribute to >70,000 diabetic limb amputations performed annually in the US (16). Hence, there is an urgent need to identify new therapies against *Pa* wound infections.

Bacteriophages (phages) are viruses that infect bacteria (17). Phages were first used to treat infections over 100 years ago (18), but the advent of antibiotics relegated phage therapy to the sidelines (19). The rise of MDR pathogens has renewed interest in phages (19). Phages have several advantages as a treatment option against MDR *Pa* infections for several reasons, including: 1) their high specificity toward their target bacteria without perturbing the host microbiome (20); 2) their potential to disrupt biofilms(21); 3) their “generally recognized as safe” status by regulatory agencies, and multiple studies showing evidence of phage safety (22–25). However, phages have a short half-life of less than half an hour in circulation after intravenous administration (26,27), suggesting localized delivery is preferable (28–30). Yet, few studies have compared the effectiveness of intravenous phage treatment to topical treatment against chronic wound infection, and current methods for topical phage delivery are insufficient.

In clinics, locally administered phage treatments for chronic wounds have had variable success, and there is no consensus on the phage concentration and frequency to use. The total phages given can be varied from $2x10^3$ to 10^{12} plaque-forming units (PFU) for wound treatment, at a daily frequency or even every couple of hours up to several weeks (31–34). Wounds are sometimes irrigated with phage-containing saline, but this approach can limit the duration of phage contact with the bacterial target, as phage-saline may easily leak out of the wound space (34). Patients are sometimes treated with wound dressings soaked with phage-saline (34). This is also suboptimal; gauze dressings can become full of exudative material and can be colonized by bacteria, and phages may adsorb irreversibly to cellulose fibers or lose bioactivity when the gauze dries up (35). Thus, frequent replacement of the dressings may be required (as often as daily or every other day). Instead, ideal phage therapy should integrate seamlessly into patients’ chronic wound care regimens, in the form of an advanced dressing that can adhere to the skin and deliver effective local concentrations of therapeutics for a week, the timescale over which these patients would typically return for treatment.

Hydrogels are attractive as wound dressings and as platforms to enable controlled topical phage delivery. Previous attempts have been made to deliver phage via hydrogels (36–38). Simply embedding phages in static, ionically crosslinked hydrogels often release most phages within 24 hours (39–41), which is insufficient for resolving chronic infections. Fibrin glues, while allowing release over longer times, offer no control over release kinetics and require shaking at high speed (42). Despite some case reports suggesting that sustained release of phages can be achieved using dressings or bandages soaked with phages, and that this is important for the clearance of infections in chronic wounds (28,29,43), the characterization of phage release kinetics have not been reported. Hence, rational design of hydrogel and systematic evaluation of treatment efficacy are needed for the advancement of phage wound treatment delivery.

To address these deficiencies, we hypothesize that topical sustained release of phages from a hydrogel can enhance the clearance of chronic wound infection, relative to systemic therapy. In this study, we developed an innovative hydrogel system called HydroPhage, and investigated its phage release kinetics and antimicrobial capability. Our data showed that HydroPhage can encapsulate phages at concentrations up to 10^{11} PFU/mL and release phages at concentrations at no less than 10^9 PFU/mL daily over a week, with more than 60% total phage released. HydroPhage significantly reduces bacterial loads in planktonic and biofilm cultures of bacteria *in vitro*. Importantly, our data showed HydroPhage improved bacterial

clearance in a novel delayed treatment murine wound infection model, and the necessity of localized and high-dose or frequent administration for the success of phage therapy. Overall, this work demonstrated HydroPhage can deliver phages topically over 1 week and enhance bacterial clearance in a wound model.

Results

Dual-crosslinking HA and PEG based hydrogel is injectable

We developed a soft and injectable hyaluronic acid (HA) and polyethylene glycol (PEG)-based hydrogel, specifically engineered to be compatible with extremely fine-gauge needles for precise application (**Fig. 1a**). This hydrogel is synthesized through a dual-crosslinking mechanism involving both covalent and dynamic covalent bonds. The covalent thioether bonds are formed between hyper-branched PEG-acrylate (HBPEG) and thiolated-hyaluronic acid (HA-SH), while dynamic covalent hemithioacetal linkages are created using 4-arm PEG-aldehyde or PEG-benzaldehyde crosslinkers (4ALD and 4BLD) that react with the thiols on HA-SH (**Fig. 1b**). These reactions occur spontaneously under physiological conditions, eliminating the need for harsh solvents or catalysts. The fast kinetics of dynamic covalent crosslinking (DCC) enables immediate enhancement of viscosity and stickiness without compromising injectability (**Supplementary Fig. 1a-b**). These features ensure easy application and secure adherence of the hydrogels to the irregular contours of infected wound surfaces. Lytic phages, for example the antipseudomonal phage PAML-31-1 (**Fig. 1c**), can then be encapsulated in the hydrogel during the mixing of polymers and crosslinkers. Overall, the unique combination of viscous, sticky, slow gelling, and exceptional injectability, enhanced by both covalent and dynamic covalent crosslinking, makes this HA-PEG hydrogel particularly suitable for application to wound beds, offering ease of use and effective delivery of therapeutic agents.

The HA-PEG hydrogel enables sustained release of high-titer phages

To develop a hydrogel formulation that enables sustained release of phages, we examined the impact of each polymer component on phage release. Release phage titers were quantified by forming hydrogels within transwell inserts, immersing these in a minimal amount of buffer, and measuring the phage titer in the buffer combined from the basolateral and apical chambers before daily transfer to a new well containing fresh buffer (**Fig. 1d**). Previous study has shown that hydrogels formed via thiol-Michael addition require polymer degradation mechanisms, like protease-cleavable crosslinkers, to facilitate phage release (44). We hypothesized that by utilizing a lower thioether crosslinking density, we could enhance phage release due to a looser polymer mesh and eliminate the need for additional polymer degradation mechanisms. Indeed, hydrogels with higher HBPEG concentrations showed reduced phage recovery, suggesting denser covalent thioether crosslinks trapped phages and limited phage release (**Supplementary Fig. 2a-c**). Further investigation into low thioether crosslinking (1 mg/mL HBPEG) revealed that higher concentrations of 4ALD and 4BLD crosslinkers led to increased percent phage recovery (**Supplementary Fig. 3a**). This effect likely resulted from the limited availability of free thiols on HA-SH, which increased the mobility of aldehyde crosslinkers that tethered the phages. At high concentrations of 4ALD and 4BLD, a lower percentage of benzaldehyde (BLD%) crosslinkers corresponded to higher percent phage recovery and more sustained release from day 4 to 7. We suspected the more stable polymer-polymer and polymer-phage bindings with benzaldehyde versus aldehyde may limit phage release. The optimal HA-PEG hydrogel formulation was thus determined as: 5 mg/mL HA-SH, 1 mg/mL HBPEG, and 75 mg/mL of 4-arm PEGs with 10% 4BLD and 90% 4ALD. This formulation was used for the rest of the study.

Next, we investigated how different characteristics of encapsulated payload affected the release kinetics. Surprisingly, higher encapsulated phage titers led to increased percent phage recovery; encapsulating 10^{11} PFU/mL in hydrogel resulted in an 87% increase in phage recovery compared to encapsulating 10^{10} PFU/mL, and a 2.5-fold increase compared to encapsulating 10^{9} PFU/mL (**Fig. 1e**). This suggests that higher titers may saturate the binding between aldehyde and free amines on the phage capsid, allowing a larger portion of unbound phages to diffuse more freely. Last, we demonstrated the slow release of three distinct *Pa*-targeting phages—Luz24, PAML-31-1, and LPS-5—from the hydrogel (**Fig. 1f**). This capability underscores the potential of our HA-PEG hydrogel to deliver a broad spectrum of phages, or a cocktail of phages, tailored to specific infections. In contrast to an ionically crosslinked alginate (AG-Ca^{2+}) hydrogel, which exhibited burst release of nearly all encapsulated phages within the first 24 hours, our HA-PEG hydrogel exhibited sustained high-titer phage release (~10^{9} PFU/mL or higher) for up to 7 days (**Fig. 1g**). The rapid depletion of phages from the AG-Ca^{2+} hydrogel is similar to the kinetics reported in most of the previous hydrogel- or microparticle-based phage delivery literature(45–56).

Finally, we examined the mechanisms mediating release of phage from the hydrogel. While the dynamic imine bonds could in principle delay phage release from the gels, leading to sustained release, varying

these bonds did not have a strong effect on release. In contrast, there was a close correspondence between the released phage percentage and the extent of polymer mass loss (**Fig. 1h**). Thus, hydrolytic erosion appears to be the primary driver of phage release from HA-PEG hydrogels. Overall, our dual-crosslinking HA-PEG hydrogel offers a novel and effective approach for the sustained delivery of high-titer phages to treat wound infections.

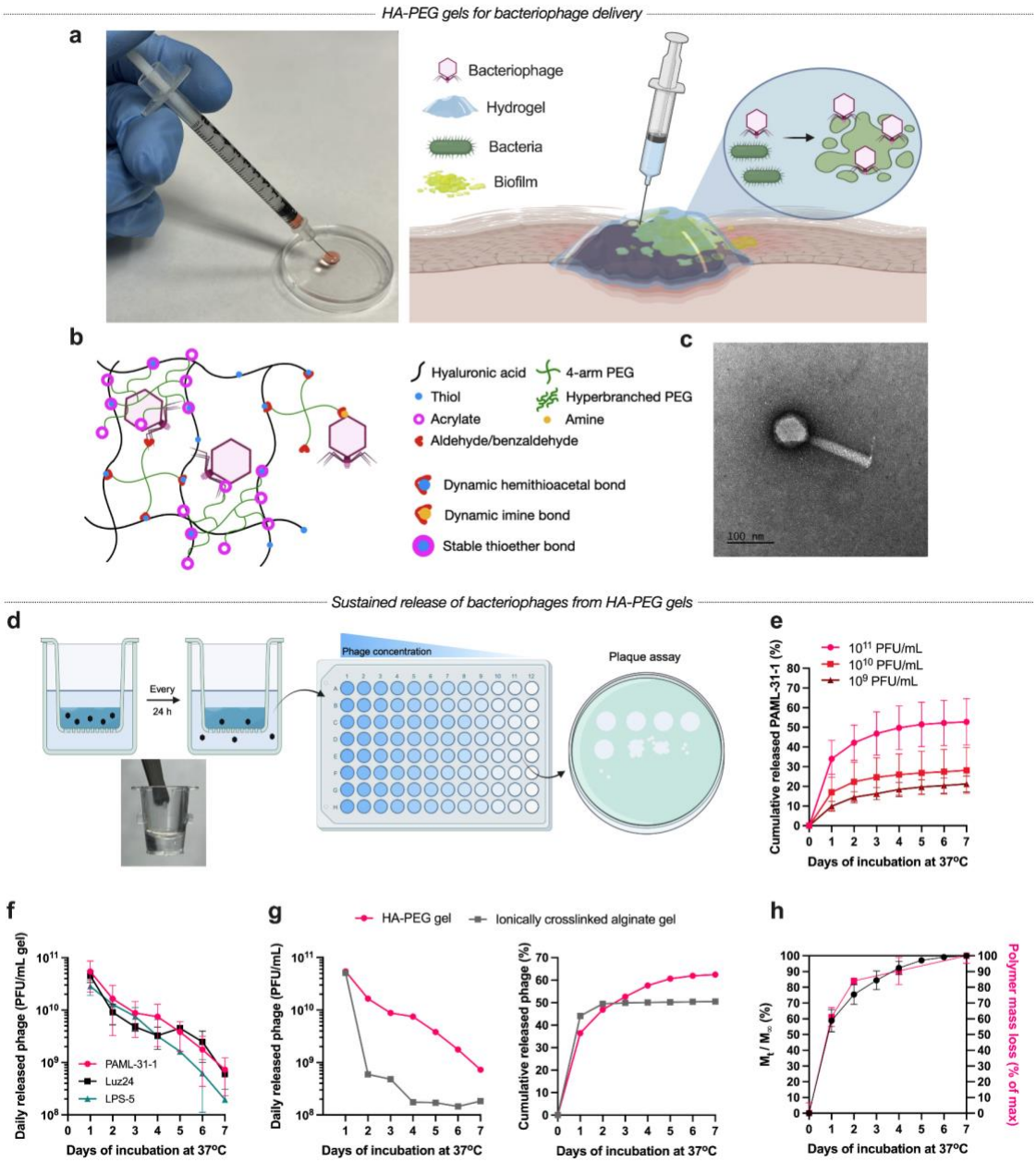

Fig. 1 HydroPhage is a dynamic covalent crosslinked hydrogel for sustained and topical delivery of high-dose bacteriophage. a, Image of hyaluronic acid (HA) and polyethylene glycol (PEG) based hydrogel (HA-PEG) injected through a 28G needle; schematic of phage release from injectable hydrogel to combat bacteria and biofilm. **b**, Schematic of HA-PEG hydrogel crosslinking chemistries. Covalent thioether crosslinks are formed between thiolated-HA (HA-SH) and hyperbranched PEG multi-acrylate (HBPEG). Dynamic covalent hemithioacetal crosslinks are formed between HA-SH with either 4-arm PEG-aldehyde (4ALD) or benzaldehyde (4BLD). Amines presented on the surface of phages could theoretically bind to aldehyde/benzaldehyde through dynamic covalent imine bonds. **c**, The transmission electron microscopy

(TEM) image of PAML-31-1 phage. Scale bar = 100 nm. **d**, Schematic of the transwell-release assay to quantify phage release from HA-PEG hydrogel daily. **e**, Quantification of cumulative release of different titers—10^{11}, 10^{10}, and 10^{9} PFU/mL—of PAML-31-1 phage out of HA-PEG hydrogel. **f**, Quantification of daily release of different phages—Luz24, PAML-31-1, and LPS-5—from HA-PEG hydrogel. **g**, Comparison of daily and cumulative release of phage from HA-PEG hydrogel and ionically crosslinked alginate hydrogel (AG-Ca^{2+}). **h**, Close correspondence between the percentage of maximum phage release, defined as the ratio of cumulative phage release at given time point (M_t) to the endpoint maximum cumulative release (M_∞), and the mass loss of HA-PEG hydrogel, defined as the percentage of mass loss to the maximum mass loss. Schematic in (**a**), (**d**) generated with bioRender.

PAML-31-1 phage effectively suppresses planktonic *Pa*

As the HA-PEG hydrogels demonstrated the capability to deliver multiple *Pa* phages at high titers in a controlled and sustained manner, we next sought to identify the most effective phage against *Pa* Xen41, a bioluminescent strain of *Pa*. To identify the most effective phage against Xen41 in planktonic growth conditions, a planktonic suppression assay (PSA) was conducted. In this assay, Xen41 was grown in liquid media either without phage (positive control) or mixed with various phages (PAML-31-1, LPS-5, Luz24, or OMKO1) at a multiplicity of infection (MOI) of 8,000, then incubated with shaking for 48 hours at physiological temperature (37 ^{o}C) with continuous measurements of optical density at 600 nm (OD600). The addition of a thin layer of mineral oil on top of each phage-bacteria mixture in each well minimized evaporation from the 96-well plate and enabled extended measurement of bacterial growth and phage resistance dynamics. PAML-31-1, which specifically targets lipopolysaccharide (LPS) in the outer membrane of *Pa*, showed the most substantial suppression of Xen41 among the tested phages. This was evidenced by a delayed onset of resistance and compression of the OD600 curve, which was quantified as the "Suppression Index" (SI%) (**Fig. 2a, b**) (57). LPS-5, which also targets *Pa* LPS, demonstrated comparable efficacy to PAML-31-1 in the PSA. Subsequent tests of PAML-31-1 and LPS-5 involving different MOIs revealed that an MOI of 8,000 was necessary for effective suppression. Only this MOI achieved a SI% greater than 80%, without bacteria densities rebounding to control level in 48 hours (**Supplementary Fig. 4a-d**). Of note, PAML-31-1 at MOI of 0.08 still achieved nearly 50% suppression. In contrast, bacterial densities were nearly unaffected by LPS-5 at MOI of 80 or below. We concluded that PAML-31-1 is most effective against planktonic *Pa* among these different phages. These results suggested high phage titer may be required to achieve good efficacy *in vivo*, especially in the context of further complications such as biofilm, phage-neutralizing antibodies, and rapid clearance (31,58,59).

Next, to contextualize the suppression capability of the phage released daily from the HA-PEG hydrogel encapsulating 10^{11} PFU/mL, we evaluated the SI% achieved by the amount of PAML-31-1 released daily from this gel. Remarkably, at least 30% suppression of planktonic *Pa* was observed for up to 7 days (**Fig. 2c**). This prolonged suppression underscores the potential of the HA-PEG hydrogel to control bacterial burdens *in vivo*.

HydroPhage disrupts *Pa* biofilms

While we demonstrated that phages can effectively suppress planktonic *Pa* in co-culture, this does not necessarily imply that phages can significantly reduce bacterial burdens *in vivo*, particularly in the presence of biofilms and immune responses(60). Biofilms are dense polymeric matrices that harbor both actively growing and dormant bacterial populations, diminish the efficacy of antimicrobials and complicate treatment outcomes (61–64). To better predict *in vivo* bacterial clearance, we explored the efficacy of phages, both free or encapsulated in the HA-PEG hydrogel, against bacteria immobilized on agar or grown in biofilm. First, we assessed the efficiency of plaquing (EOP) of various phages against the Xen41 compared to its parent strain, PAO1. PAML-31-1 showed less than a one-log reduction in EOP against Xen41 versus PAO1, whereas Luz24 and OMKO1 were significantly less effective against Xen41 versus PAO1, showing three- and five-log reductions in EOP respectively (**Fig. 2d**). Notably, LPS-5 exhibited markedly reduced plaquing efficiency when assessed on agar plates than might be predicted based on its relatively stronger suppression of planktonic Xen41 compared to Luz24 and OMKO1, with a six-log reduction in EOP. These findings hint that phages effective against planktonic bacteria may not exhibit the same efficacy against bacteria grown on a semi-solid substrate. Consequently, we encapsulated PAML-31-1 in our HA-PEG hydrogel, a combination henceforth called "HydroPhage".

We then tested whether PAML-31-1 could still escape the hydrogel and lyse *Pa* grown on a semi-solid substrate, even when the hydrogel was not submerged in fluid as we had previously tested. To test this, we measured the zone of inhibition (ZOI) produced by HydroPhage relative to empty hydrogel on Mueller-Hinton agar plates inoculated with *Pa*, finding that HydroPhage caused a 60% increase in the ZOI relative to empty hydrogel (EG), indicating that released phages could not only escape the hydrogel under drier conditions than previously tested, but also that they could infect and propagate beyond the area in direct contact with the hydrogel (**Fig. 2e, f**).

Thus far, we had evaluated the efficacy of phages and HydroPhage in co-culture with bacteria. To assess the efficacy of PAML-31-1 against established biofilms, we inoculated PAO1-GFP on the surface of top

agar in a multi-well plate, allowed biofilms to grow for 24 hours, and then treated the established biofilms either with PAML-31-1 added directly to the surface, or with HydroPhage or an empty hydrogel (EG) in a transwell insert. Both PAML-31-1 and HydroPhage disrupted established biofilms, with reductions in biofilm thickness of 43% and 52% at 21 hours, respectively, relative to pretreatment. No disruption of biofilm growth was observed with the empty hydrogel or untreated control (**Supplementary Fig. 5a**). Furthermore, PAML-31-1 and HydroPhage decreased biofilm density by 57% and 65% respectively, whereas the empty hydrogel and control exhibited increases in biofilm density of 55% and 72% (**Fig. 2g**). Confocal microscopy vividly illustrated the undisrupted densifying biofilm under treatment with EG and control and the marked to complete disruption under treatment with PAML-31-1 in media and PAML-31-1 released from the hydrogel (**Fig. 2h, i and Supplementary Fig. 5b**). In conclusion, HydroPhage (PAML-31-1 released from the HA-PEG hydrogel), effectively suppresses and disrupts *P*a across planktonic and biofilm conditions.

HydroPhage is biocompatible and nonimmunogenic to macrophage-like cells

Having demonstrated the antibacterial properties of HydroPhage, we next conducted *in vitro* toxicologic studies to assess the biocompatibility and immunogenicity of HydroPhage. We cultured monolayers of RAW264.7 murine macrophage-like cells and incubated the monolayers for 24 hours at 37 ^{o}C with HydroPhage in transwell inserts (**Supplementary Fig. 6a**). We found that HydroPhage did not exert any cytotoxicity to RAW264.7 cells (**Supplementary Fig. 6b**). We also used flow cytometry to assess if HydroPhage polarized RAW264.7 cells towards M1 or M2 phenotypes, by measuring expression of canonical M1 (CD80, CD86) or M2 (CD163, CD209) markers. We found no upregulation of these markers in response to treatment with HydroPhage (**Supplementary Fig. 6c-j)**. These data suggested that HydroPhage may be suitable for use *in vivo*.

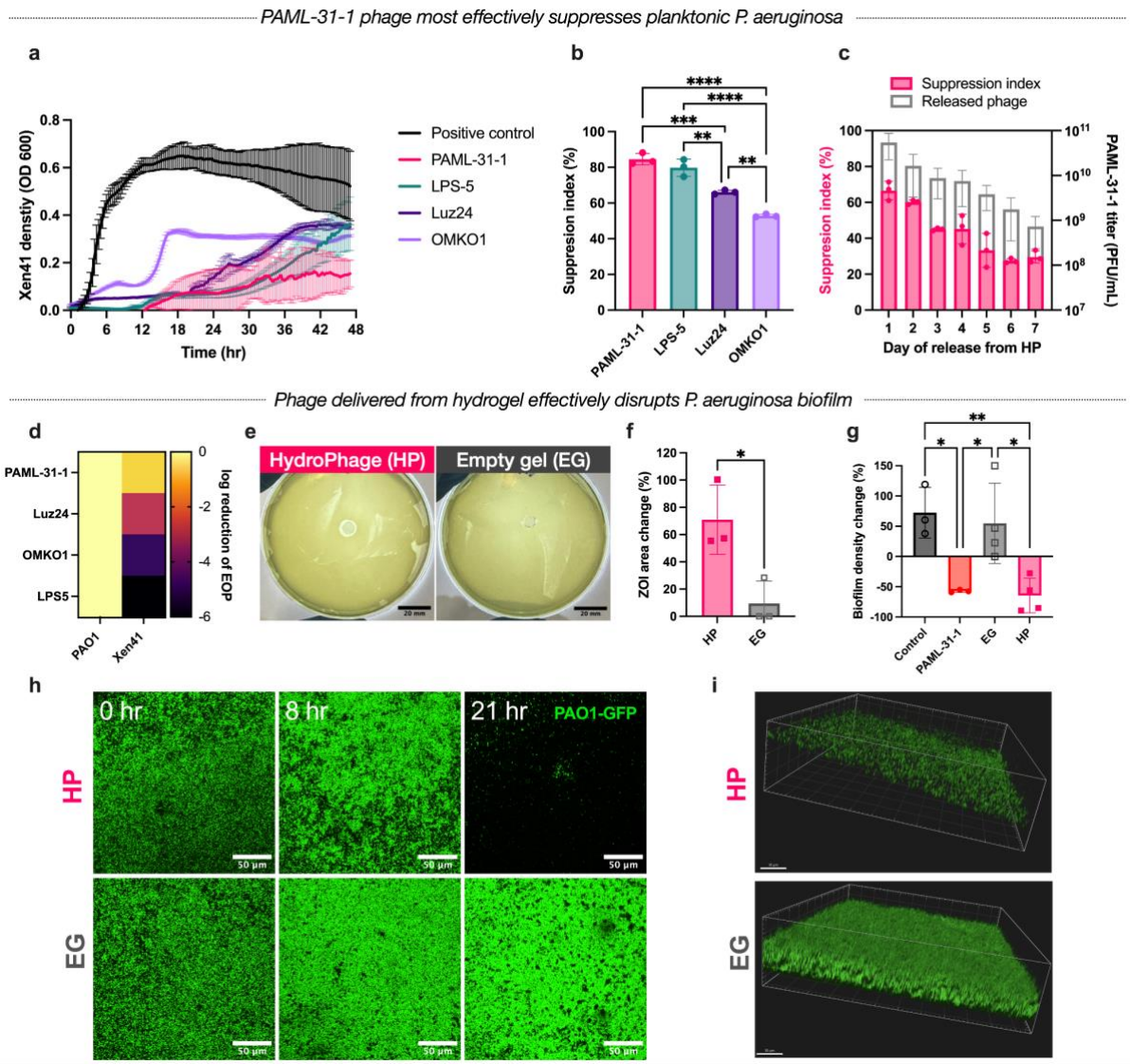

Fig. 2 High-dose PAML-31-1 is effective against *Pseudomonas aeruginosa* in planktonic and biofilm conditions. a,**b**, Different phages—PAML-31-1, LPS-5, Luz24, and OMKO1—were co-culture with Xen41 in planktonic condition at the multiplicity of infection (MOI) of 8,000 with shaking for 48 hours and monitored every 20 minutes. Time evolution of optical density at 600 nm (OD600) (**a**), and the quantification of bacterial suppression by suppression index (SI%) (**b**) (n=3 each). **c**, Quantification of SI% of the titer of PAML-31-1 released from HA-PEG hydrogel in transwell-release assay daily. **d**, The efficiency of plaquing (EOP) was quantified by comparing the log reduction of plaque counts of different phages on Xen41 versus its parent strain PAO1. **e**,**f**, The zone of inhibition (ZOI) formed by HydroPhage (HP) and empty gel (EG) at 24 hours of gel placement on *Pa* lawn. The representative images of HP and EG on *Pa* lawn (**e**), and quantification of change in ZOI area at 24 hours as a percent of initial area of hydrogel (**f**) (n=3, unpaired two-tailed Student's t-test). **g**,**h**,**i**, PAO1-GFP biofilm was formed on the surface of top agar and treated with media control, PAML-31-1 phage in media, EG or HP for 21 hours. The quantification of biofilm density changes (**g**) (n=3 each), representative confocal images (**h**) of biofilm incubated with HP and EG treatments over hours, and their 3D rendering (**i**). Scale bars: 20 mm for (**e**), 50 µm for (**h**), and 30 µm for (**i**). Data are mean ± S.D.

Localized HydroPhage treatment enhances the clearance of infection from murine wounds

After demonstrating the efficacy of HydroPhage *in vitro* and its ability to disrupt biofilms, we wanted to test the *in vivo* efficacy of HydroPhage in a model designed to closely mimic the clinical parameters of wound care for patients with chronic wound infections. Thus, we developed a mouse wound infection model with delayed treatment. In contrast to other murine wound infection models, which introduce phage treatments within a few hours of or even along with bacterial inoculation, we delayed phage treatment to mice 24 hours post-infection (**Fig. 3a**). In this model, *in vivo* bioluminescence imaging (BLI) is used to monitor the infection of PAO1-derived luminescent Xen41 and efficacy of treatment daily. Importantly, bacterial colony-forming units (CFU) correlated with luminescent flux *in vitro* and *in vivo* (**Supplementary Fig. 7a, b**). To identify the appropriate Xen41 inoculum, mice were inoculated with a range of bacterial burdens from 1 x 10^5 CFU/wound to 3.7 x 10^6 CFU/wound, and were then assessed for whether they carried the infections after 24 hrs. 5 x 10^5 CFU/wound represented the minimum inoculation dose that resulted in a 100% infection rate, and was therefore used as the inoculation dosage in experiments (**Fig. 3b**).

We hypothesized that localized phage treatment would enhance the clearance of infection from wounds compared to systemic treatment. To test this, mice were treated with HydroPhage (HP) as topical injections (**Fig. 3c**) or with intravenous injection (IV) of the same total amount of phage under a layer of Tegaderm. Bacterial burden in wounds was monitored daily using BLI (**Fig. 3d**). The percentage of wounds with bioluminescent flux lower than the detection of limit (LoD) was used as a measure of clearance of infection. This quantification indicated that treatment with HP was superior to treatment with IV injection (**Fig. 3e**). Mice treated with HP had a 40% clearance rate at the end of the study on Day 6 post-infection, compared to merely 6% for mice treated with IV injection (**Fig. 3f**). At the end of the experiments, wound tissues were harvested, homogenized, plated, and counted for CFUs and PFUs. Although similar amounts of phages were found in the wound homogenates in HP- and IV-treated mice (**Fig. 3g**), HP demonstrated far superior antimicrobial efficacy compared to IV and PBS control (**Fig. 3h**), with a >2-log reduction in CFU/mg wound tissue relative to PBS for HP-treated mice (2.15, n=20) compared to a <1-log reduction in CFU/mg for IV-treated mice (0.72, n=20). The eradication rate, defined as a CFU/mg measurement at or below the LoD, was then quantified for each treatment. CFU assays demonstrated similar improvement in eradication in HP relative to IV as the BLI measurements: HP treatment eradicated 25% of infections in mice, compared to just 5% for IV treatment (**Fig. 3i**). Together, our results suggest that the localized delivery of phages via HA-PEG hydrogel with PAML-31-1 phages (HP) results in enhanced clearance and superior eradication of *Pa* from murine wounds than systemic therapy (IV).

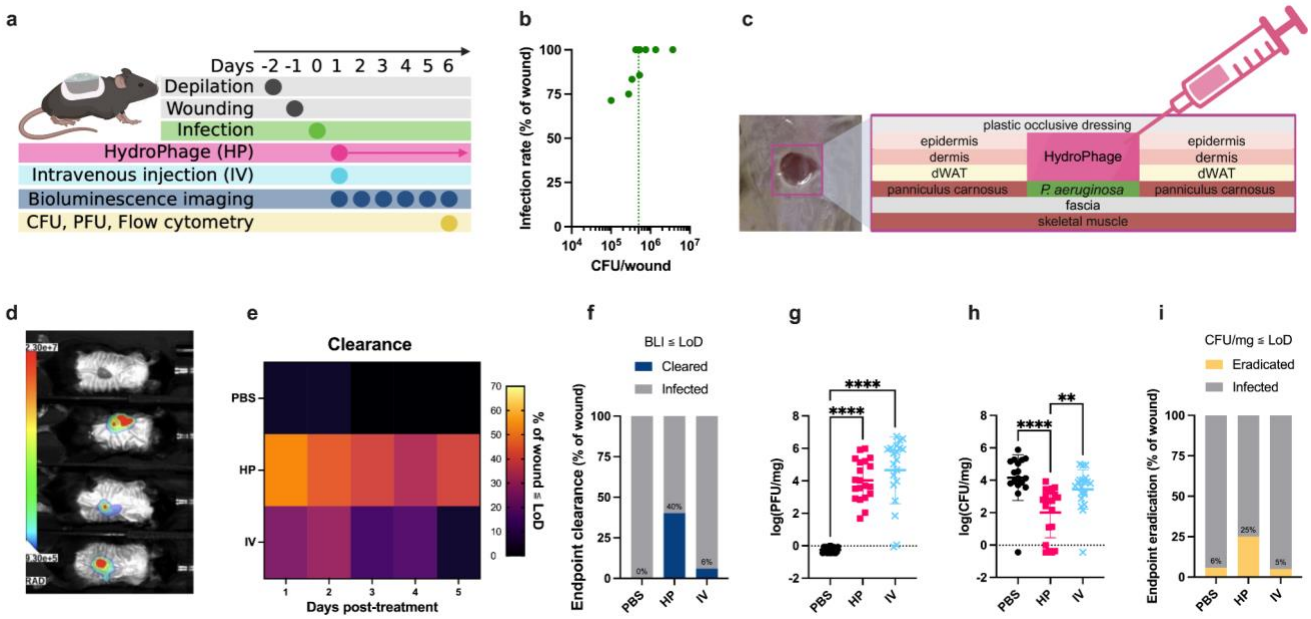

Fig. 3. Localized HydroPhage treatment clears infection from murine wounds. a, Illustration of a murine wound infection study to test the efficacy of HydroPhage (HP) and intravenous (IV) injection

treatments. **b**, The wound infection rate at different inoculation density of Xen41. **c**, Representative image of full-thickness wound created on the back of a C57BL/6J mouse covered by semi-occlusive dressing Tegaderm (left); the schematic of tissue layers in mouse skin and demonstration of HydroPhage injection directly under Tegaderm and above the established *Pa* infection. **d**, Representative *in vivo* bioluminescence (BLI) image of mice without infection (top) and with infection (bottom three) colored by the intensity of Xen41 flux (photons/sec). **e**, The heatmap presents the daily calculated percentage of wound infection clearance, defined as bioluminescent flux lower than the limit of detection (LoD). **f**, Percentage of wound infection clearance at the end of the study, day 5 post-treatment (n=17 for PBS, n=15 for HP, and n=17 for IV). **g**,**h**,**i**, Endpoint characterization of harvested mice wound tissue. Phage counts (PFU/mg) (**g**) and bacterial burden (CFU/mg) (**h**) recovered, and the eradication rate defined as the percentage of wounds having bacterial burden (CFU/mg) below limit LoD (**i**) (n=17 for PBS, n=20 for HP, and n=20 for IV). One-way ANOVA with Tukey's post-hoc test for (**g)** and (**i**). (** $P \leq 0.01$, **** $P \leq 0.0001$). Schematic in (**a**), (**c**) generated with bioRender.

High-dose and repeated phage exposures reduce bacterial burden

After demonstrating that localized HP phage treatment was more effective in controlling bacterial burden than systemic therapy through IV, we investigated how phage dosing concentration and frequency influenced treatment efficacy. We hypothesized that higher concentration of phage or more frequent administrations would enhance bacterial clearance compared to lower concentrations of phage or single-dose treatment. To evaluate this, we first compared the efficacy of two different phage doses: a single high-dose (HD, 1 x 10^{11} PFU/mL) and single low-dose (LD, 2.5 x 10^{10} PFU/mL) (**Supplementary Fig. 8a, b**). Daily BLI results showed that HD clears bacteria more effectively than LD, indicating that a higher topical dose is more effective to reduce bacterial burden in wounds (**Supplementary Fig. 8c**). Next, the impact of dosing frequency was assessed by comparing a regimen of daily low-dose for four days (DD, 2.5 x 10^{10} PFU/mL/day) to a single low-dose (LD). , ,r , (**Supplementary Fig. 8c, d**). The total amount of phage in the wound homogenate was similar between treatment groups, regardless of the differences in treatment dosage and frequency (**Supplementary Fig. 8e**). Analysis of CFU/mg at the end of experiments supported the conclusions derived from BLI. Relative to PBS control treatment, mice treated with DD (n=14) or HD (n=11) presented higher log reduction in CFU counts compared to LD (n=19), with 2.20-, 2.16- , and 1.44-log reductions in CFU/mg at the end of the study, respectively **(Supplementary Fig. 8f)**. Comparing eradication rates suggested strong performance of the daily dosing strategy, with 29% eradication rate in mice receiving daily treatment versus 18% in the single high-dose group (HD) and 16% in the single low-dose group (LD). (**Supplementary Fig. 8g**). By multiple measures, our data support the conclusion that daily treatment with phage reduces bacterial burdens and clears wounds of bacteria more effectively than the same total amount of phage given as a single high dose, and that a single high dose is better than a single low dose. Overall, our data suggest that high local concentration or repeated phage treatments enhance bacterial clearance and eradication.

Changes of skin-associated immune cell population are infection and treatments dependent.

Our *in vitro* studies previously showed that HydroPhage was not intrinsically cytotoxic or immunostimulatory to RAW264.7 cells **(Supplementary Fig.6)**, but it remained plausible that HydroPhage or other phage treatments affected the local immune response and/or the abundance of specific cell types in the skin *in vivo*. We therefore assessed the local immunologic response to *Pa* wound infection and how this was affected by phage treatments, including HydroPhage, by quantifying the abundance of myeloid and adaptive immune cells in the skin at the end of the infection study (**Supplementary Fig. 8a**). A flow cytometry panel with 13 labels (**Supplementary Table 2**) was used to discriminate most major myeloid cell populations in the skin. After gating on singlet, live, $CD45^+$ cells, lineage-positive cells (natural killer cells, B cells, and T cells) were excluded in order to identify neutrophils, macrophages, monocytes, monocyte-derived dendritic cells (MoDCs), and conventional dendritic cells (cDCs) (**Supplementary Fig. 10**). Apart from natural killer cells, subpopulations of innate lymphocytes were not discriminated in the downstream gating.

Infection with *Pa* caused several robust changes to the immune cell composition of mouse wounds on Day 6 post-infection. We observed a significantly increased proportion of $CD45^+$ cells and natural killer cells, and a trend towards increased neutrophils. We also observed a significant reduction in proportion of T cells,

possibly suggesting T cell death caused by *Pa* infection, but no changes in the abundance of skin-associated B cells **(Supplementary Fig. 11)**. Successful treatment with HydroPhage or other phage treatments were partly able to reverse these effects, with decreases in $CD45^+$ cells, NK cells, and neutrophils following successful treatment. However, we did not observe a restoration of the depleted population of cutaneous T cells following successful treatment **(Supplementary Fig. 12)**.

Thus, immune profiling shows several infection-dependent changes in the abundance of skin-associated immune cell populations and that successful treatment with HydroPhage, or other liquid phage treatments can revert some of those changes.

Development of PAML-31-1 resistance is independent of treatment dosage, route, and efficacy

Our wound model results demonstrated that various treatment dosages, frequencies, and delivery routes resulted in different levels of bacterial burden reduction and/or clearance/eradication. Interestingly, despite their differences, all treatments shared some common results, including increased proportion of wounds with detectable bioluminescence signal on later days post-treatment compared to earlier days post-treatment (**Fig. 3e and Supplementary Fig. 8c**) and endpoint eradication rates that did not exceed 30%, despite the use of high-titer phages (**Fig. 3i and Supplementary Fig. 8g**). To explain these results, we hypothesized that bacteria might develop resistance against phages *in vivo* if not fully eradicated, similar to behavior observed in the platonic suppression assay (PSA) (**Fig. 2a and Supplementary Fig. 4a, c**). The positive correlation between phage and bacteria counts at the endpoint suggested that persisting bacterial burdens were not due to phage depletion (**Supplementary Fig. 9**). To confirm that resistance to PAML-31-1 had developed *in vivo* in response to PAML-31-1 phage treatments, a PSA with overnight cultures of bacterial isolates from our *in vivo* experiments were challenged with PAML-31-1 phage was conducted. Bacterial isolates from all treatment groups except the phage-unexposed PBS control, exhibited significant reductions in suppression index (SI%) compared to phage-unexposed wild-type Xen41, indicating that resistance had developed even with ineffective treatments such as IV injection (**Fig. 4a**). The comparable SI% among treatments indicated the development of resistance was independent of the treatment efficacy. To summarize, these results demonstrated that resistance against PAML-31-1 developed regardless of treatment dosage, frequency, delivery route, and was not correlated with the reduction of bacterial burden.

While resistance to PAML-31-1 could be anticipated, since treatment with PAML-31-1 would select for resistant populations, it remained unknown whether resistance would arise to another phage that infects *Pa* using a different receptor. Therefore, we conducted PSA on mice isolates but challenged them with Luz24 phage, which targets type IV pili of bacteria, as opposed to LPS used by PAML-31-1. Unexpectedly, isolates from all treatments, including the PBS control, presented a decreased mean SI% against Luz24, with no significant change for PBS, HP, and HD (**Fig. 4b**). This indicated that bacteria might undergo spontaneous mutations *in vivo*, altering the expression of type IV pili over time. Notably, daily low-dose (DD) treatment and less effective treatments, such as LD and IV, exacerbated the development of resistance, as indicated by significantly lower SI% compared to wild-type Xen41 and instances of complete resistance (i.e., SI% of 0). Surprisingly, among all localized phage treatments, HydroPhage did not lead to any complete resistance against Luz24 and showed a significantly higher suppression than DD (**Supplementary Fig. 13**).

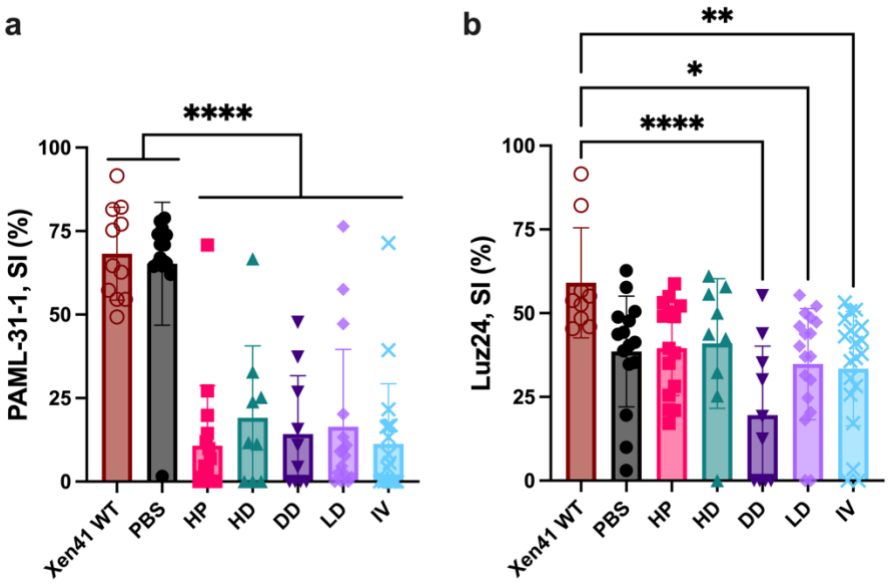

Fig. 4. Development of phage resistance is independent of treatment, dosing, route, and efficacy. a, b, Planktonic suppression assay (PSA) for the mice wound isolates to characterize bacteria resistance against phages after PBS control and PAML-31-1 treatments. **a**, Quantification of suppression index (SI%) of PAML-31-1 against wound isolates. **b**, Quantification of suppression index (SI%) of PAML-31-1 against wound isolates. **c**, Quantification of suppression index (SI%) of Luz24 against wound isolates. One-way ANOVA with Tukey's post-hoc test. (* $P \leq 0.05$, ** $P \leq 0.01$, *** $P \leq 0.001$, **** $P \leq 0.0001$)

Discussion

We introduce "HydroPhage" (HP), a novel hydrogel system designed for the sustained delivery of high-titer bacteriophages to treat multidrug resistance (MDR) wound infections. Through dual-crosslinking of HA-PEG hydrogel with static covalent and dynamic covalent bonds, this system encapsulates phages effectively while maintaining superb bioactivity, releasing them in controlled doses over an extended period. The localized HP approach has shown superior bacterial eradication over intravenous (IV) phage injection in a preclinical murine model despite the emergence of phage resistance. Furthermore, this work underscores the importance of maintaining high local phage concentration and frequent dosing to manage wound infection efficiently. Thus, HP represents a significant advancement in the topical treatment of chronic infections.

The management of chronic wound infections poses significant challenges, particularly with the rise of MDR pathogens like *Pa*. Current wound infection management often fails to eradicate these infections, despite aggressive measures including debridement, systemic and topical antibiotics, and various dressings to control moisture (65). The protective environment of biofilms often complicates the treatment outcome, the rapid development of resistance, the lack of bandwidth from clinics and physicians for frequent assessment, and the morbidity of the wounds, which limits patients' capacity to adhere to at-home care practices(66,67). Despite the recognized potential of phage therapy (PT) for treating resistant infections, developing suitable wound dressings tailored for topical phage delivery, supported by proven preclinical models, has lagged. Due to their intrinsic viscoelasticity and injectability, DCC hydrogels have gained significant attention in many biomedical applications (68–73). Among various DCC chemistries considered, hemithioacetal crosslinking seemed ideal for making hydrogels for topical application, as the rapid kinetics could provide immediate enhancement of viscosity and the lower equilibrium constant may enable easy spreading and injectability (74,75). We leveraged these properties from hemithioacetal crosslinks combined with the stability of covalent thioether bonds, to develop an adherent slow-gelling hydrogel (**Supplementary Fig.1b**). Our dual-crosslinking hydrogels are easily injectable (**Supplementary Fig.1a**) and can contour the uneven wound bed to provide prolonged contact of the therapeutic with the affected area. The low covalent thioether crosslinks density provides the necessary stability but is not too dense to trap sub-micron scale particles and allows hydrolytic erosion to release phages from the HA-PEG hydrogel in a more sustained manner (**Fig. 1e-g**). The ability to further accelerate erosion for ease of dressing removal through disrupting hemithioacetal linkages by thiol-containing molecules, further highlighting the translational potential of this class of hydrogel to deliver therapeutics, such as phages, to tackle topical wound infections.

Selecting the appropriate phage and appropriate animal model and endpoints is crucial to evaluating the potential for successful PT. To ensure this, we highlight several factors of our approach. First, our choice of phage was informed by assessing bacterial suppression in both planktonic (**Fig. 2a, b)** and semi-solid mediums (**Fig. 2d**). We verified the efficacy of the selected phage in the hydrogel system using the zone of inhibition (**Fig. 2e, f**) and biofilm studies (**Fig. 2g-i**), as bacteria frequently establish biofilm on chronic wounds. Second, we designed the treatment course to match clinical treatment protocols. For outpatient clinics, patients usually visit weekly to receive treatments. Hence, we extended the total study length up to 6 days post-infection (**Fig. 3a**), which allows us to test the feasibility and effectiveness of HP in integrating with clinical practice. Third, we used bioluminescent imaging (BLI) in conjunction with gold-standard culture-based assays to monitor the daily progression of infections along with the endpoint efficacy of administered treatments. We observed a high consistency between BLI and culture-based assays (**Fig. 3f, i and Fig. 8d, g**), suggesting high internal validity. Fourth, apart from bacterial clearance, we assessed several endpoints relevant to clinical translation, including the cutaneous immune response to phage treatments (**Supplementary Fig. 11, 12**) and phage resistance generation (**Fig. 4a**). These robust approaches allowed us to answer outstanding questions about the safety and efficacy of different dosing strategies with maximum external validity and translatability, using as few mice as possible.

Our findings establish the advantage of local delivery over intravenous delivery for treatment of wound infections. Previously, the benefits of topical treatments were anecdotally reported in Eastern European case studies. Researchers have also speculated that topical administration of phages would be beneficial (28,29) In addition, studies have suggested that phages either lose their activity or are cleared quickly after IV administration (26,27,76). Hence, we compared HP to IV to understand how different treatment routes

affect efficacy. Our results indicate that for the same amount of phage administered, hydrogel-enabled topical delivery leads to superior eradication than IV treatment (**Fig. 3e-i**). The correlation of recovered PFU and CFU (Supplementary Fig. 9) suggested the comparable endpoint PFU counts are likely due to propagation, and the ineffectiveness of IV is the result of a low initial concentration of phage delivered to the site of infection, evidenced by the failure of bacterial clearance from the start (**Fig. 3e**).

Next, we asked how different concentrations of phages and dosing frequency affect treatment outcomes. We first compared the treatment outcomes of a single high-dose (HD) to a single low-dose (LD). HD showed increased bacterial burden reduction during the first two days of daily monitoring compared to LD. As the infection progressed, the bacterial burden in the HD group started to rebound. At the end of the study, HD showed better bacterial burden reduction efficacy, but only slightly enhanced eradication compared to LD (**Supplementary Fig. 8c-g**). This indicates that high concentration of phage is important to suppress the initial bacterial burden but not sufficient to prevent the recurrence of infection. The comparison of daily low-dose (DD) to LD demonstrates the improved eradication of repeated dosing (**Supplementary Fig. 8c-g**), and the higher eradication compared HD with the same total amount of phages further highlights the importance of repeated exposure versus single administration. However, repeated administration of phages for outpatients is impractical. Therefore, HP presents a clinically practical approach to facilitate localized, high-dose, and sustained exposure of phage to combat wound infection.

The resistance of bacteria to phages is a common challenge in *Pa* wound infection. Our platonic suppression assay (PSA) results on mice isolates suggested resistance against phage will develop *in vivo* regardless of dosing strategies and delivering route (**Fig. 4a**). Despite resistance, we see drastic differences in bacterial burden at the endpoint and throughout the study. HP achieved comparable CFU-reduction (**Fig. 3h and Supplementary Fig.8d**) and eradication rate (**Fig. 3i and Supplementary Fig.8g**) to DD; however, HP treatment did not provoke significant resistance against another unexposed phage (**Supplementary Fig.13**). We speculate the hydrogel-enabled initial burst release followed by continuous sustained release plays a role in alleviating bacterial phenotypic changes in response to phage treatment, compared to discrete daily dosing. The inevitable rise of resistance against treatment phage and unexpected resistance to an unexposed phage, underscore the potential benefit of tracking the susceptibility of patient isolates against a broad spectrum of phages targeting different receptors, using the handful of *in vitro* assays (**Fig. 2 and 4**) described in this work.

Finally, we assessed cutaneous immune responses to *Pa* infection in wounds and how phage treatments affect such responses. *Pa* infection caused immune activation, with increased proportions of $CD45^+$ cells, NK cells (which regulate the early onset and resolution of inflammatory response in wounds (77,78), and neutrophils, which clear bacteria and are first responders in wounds (79). Among adaptive cells, we found no changes in B cells and a significant decrease in T cells (**Supplementary Fig. 11e**). Previously, our group hinted that reductions in T cells in secondary lymphoid organs during chronic *Pa* infection could be due to premature death (80). After establishing the baseline response to *Pa* infection in wounds, we evaluated if and how HP and other phage treatments attenuate this. After HP and other phage treatments, mice that remained infected had a similar immune cell composition as PBS-treated mice, with increased $CD45^+$ cells, NK cells, and neutrophils, similar B cell levels, and reduced T cell levels (**Supplementary Fig. 12**), which suggests that HP and other phage treatments did not further activate host immunity. When we compared HP-treated mice that eradicated infections versus those that did not, we found significant reductions in $CD45^+$ cells and neutrophils, suggesting that eradication can reduce infection-dependent immune activation. Lastly, exploring different phage treatment schemes revealed a similar trend (**Supplementary Fig. 12a-e, f, h**). Our results add to the growing body of evidence on the safety of phage therapy by demonstrating that phages do not provoke strong cutaneous immune responses.

To conclude, our wound infection model with complementary real-time and endpoint characterizations, underscored that localized, high-titer, and repeated dosing facilitated more effective bacterial burden management despite the inevitable rise of phage resistance.

Methods

Phage propagation

Phages were propagated using methods previously established in the lab (81). PAML-31-1, LPS-5, Luz24, and OMKO1 were propagated in *Pseudomonas aeruginosa* (*Pa*) strain PAO1. Early- to mid-log phase cultures were infected with phages to generate lysates from 300 mL cultures.

Phage purification using AKTA-FPLC system

Bacteria were removed by 2-3 rounds of centrifugation at 8000 x *g*, 10 min, 4 ºC. Supernatants were filtered through a 0.22 µm polyethersulfone (PES) membrane filter (Corning, Cat. No. 4311188). The supernatant was treated with 5 U/mL Benzonase Nuclease (Sigma-Aldrich, Cat. No. E8263) overnight to digest free DNA. Benzonase-treated lysates were then mixed with 3M KH_2PO_4 buffer (pH 7.0) in a 1:1 ratio in preparation for purification by fast protein liquid chromatography (FPLC). The FPLC-based virus purification was conducted with a CIMmultus OH 1 mL monolithic column with a 2 µm channel size (Sartorius BIA Separations, Ajdovščina, Slovenia). The washing, regeneration, performance test, and storage of the column was carried out according to manufacturer recommendations. The column was attached to an ÄKTA Pure FPLC (GE Healthcare Biosciences, Sweden) equipped with a P960 sample pump and analyzed with UNICORN 5.0 software (Cytiva Life Sciences, USA). All purification protocols were run at room temperature and all buffers and samples were filtered through a 0.22 µm PES membrane. 40-60 mL of the mixed sample was loaded onto a pre-equilibrated column with 1.5 M KH_2PO_4 loading buffer, pH 7.0. After sample loading, the column was washed with 10 column volumes of loading buffer to remove unbound particles. The elution of bacteriophage was performed using a linear gradient over 20 column volumes from 1.5M to 20 mM KH_2PO_4. The fraction corresponding to the eluted phage was collected based on UV A280 measurement. We then dilute or perform buffer exchange on the eluted phages into Tris+Mg buffer (100 mM NaCl, 50 mM Tris-HCl, 8 mM $MgSO_4$, pH 7.50).

Phage characterization

The size and morphology of phages were assessed using transmission electron microscopy (TEM) on a JEOL JEM1400 (JEOL USA Inc., Peabody, MA, USA) operating at 80 kV. In brief, 5 µL of diluted phage solution was applied onto carbon-coated copper grids (FCF-200-Cu, Electron Microscopy Sciences, Hatfield, PA, USA). Following a 3-minute incubation, the grid was immersed in ddH2O and subsequently treated with 1% uranyl acetate for staining. After drying for 15 minutes, the sample was ready for TEM imaging.

Hydrogel preparation

For making HA-PEG hydrogel, thiolated hyaluronic acid (HA-SH, 450 kDa, Blafar Ltd), hyperbranched PEG multi-acrylate (HBPEG, 10 kDa, Blafar Ltd), 4-arm PEG-aldehyde (4ALD, 10 kDa, CreativePEGWorks), and 4-arm PEG-benzaldehyde (4BLD, 10 kDa, SINOPEG) were reconstituted in PBS+Mg (Phosphate-Buffered Saline + 8 mM $MgSO_4$, pH=7.50) at concentration of 1wt%, 5wt%, 40 mM, and 40 mM respectively, adjusted to neutral pH, purged with argon gas and kept on ice before use. Appropriate volumes of the following reagents were added into an Eppendorf tube in the order of: PBS+Mg, HBPEG, 4-BLD, 4-ALD to make a crosslinker mixture. Next, phage was added to the crosslinkers and vortexed, then HA-SH was added, vortexed, and mixed thoroughly by pipetting. The viscous slow-gelling mixture then could be withdrawn by pipette to deposit into Transwell insert (Corning, USA, Cat. No. 353492) for *in vitro* assays or by insulin syringe with 28G needle (BD, REF. 329461) to inject for *in vivo* treatment. The final formulation of HA-PEG hydrogel was 5 mg/mL HA-SH, 1 mg/mL HBPEG, 75 mg/mL of 4-arm PEGs with 10% 4BLD and 90% 4ALD, and 10^{11} PFU/mL phage unless otherwise noted.

For making ionically crosslinked alginate hydrogel (AG-Ca^{2+}), lyophilized alginate (PRONOVA UP VLVG, IFF, USA) was reconstituted in Tris+Mg buffer (50 mM Tris-HCl, 100 mM NaCl, 8 mM $MgSO_4$) at 4wt%. Calcium sulfate was prepared as a form of saturated slurry in deionized water at 500 mM. Reconstituted alginate and phage solution were added to a 1 mL syringe, and calcium slurry was added into another syringe using pipette. The solution in each syringe was thoroughly mixed by moving the plunge up and down, before connecting syringes with a Luer lock. Alginate, calcium, and phages were then mixed thoroughly between syringes, then deposited 100 uL onto a Transwell insert. The formulation of AG-Ca^{2+}

hydrogel was 2wt% alginate, 50 mM calcium, and 10^{11} PFU/mL phage. Detailed polymer information was included in Supplementary Table 3.

Transwell-release assay

Transwell inserts for 24-well plates were blocked in a solution of 2% bovine serum albumin (BSA) in PBS for 1-2 hours, rinse with PBS+Mg for 10 min, then thoroughly aspirated then air-dried prior to use (20 min, covered, room temperature). 100 uL of hydrogel with encapsulated phage was aliquoted to each transwell insert and incubated in a closed box at room temperature for 3-3.5 hours until the hydrogels had fully gelled. After gelation, transwells were transferred to 24-well tissue culture-treated plates (Corning, NY, USA, Cat. No. 3524) containing 500 uL of PBS+Mg buffer. An additional 200 uL of PBS+Mg was added on top of the hydrogel to prevent drying. After 24 hours of incubation at 37 ^{o}C, the transwell insert with hydrogel was removed. The buffer on top of the hydrogel and any residual buffer on the bottom of the transwell were carefully removed and combined with the buffer in the 24-well plate and stored in 4°C for phage titer quantification. The transwell was transferred into a new well containing 500 µL of fresh buffer and 200 µL of fresh buffer was added on top. This process was repeated for 7 days.

HA-PEG hydrogel erosion

Erosion study on HA-PEG hydrogel without the phage encapsulation was performed by forming hydrogels in the transwell insert and submerged in the PBS+Mg buffer, transferred daily as described in the Transwell-release assay method section. The dry mass of hydrogel was weighed at each time point after hydrogel was lyophilized. Erosion, defined as the percentage to maximum polymer mass loss, was quantified as the loss of dry mass at each time point normalized to the endpoint of assay on day 7.

Plaque assays

Phages were enumerated by plaque assays using the spot dilution double-agar overlay technique. 100 µL of mid-log phase bacteria was added to 5 mL of top agar (5 g/L agar, 10 g/L tryptone, 10 g/L NaCl, 20 mM $MgSO_4$, 20 mM $CaCl_2$) and poured onto LB-agar plates to solidify. 10-fold serial dilutions of phages were prepared in 96-well polystyrene U-bottom tissue culture-treated plates (ThermoFisher Scientific, Waltham, MA, USA, Cat. No. 168136) in SM buffer (50 mM Tris-HCl, 100 mM NaCl, 8 mM $MgSO_4$, 0.01% gelatin (Sigma-Aldrich, USA, Cat. No. G7041), pH = 7.50). 10 µL of each dilution was spotted onto the top agar, incubated at 37 °C overnight, and plaques were counted.

Planktonic suppression assay (PSA)

Overnight cultures directly from glycerol stock of Xen41 or mice wound isolates were prepared. 50 uL of diluted overnight culture of bacteria in "modified-LB" (LB buffer + 50 mM Tris-HCl + 8 mM $MgSO_4$, pH = 7.50) were prepared at concentration of 3.75 x 10^7 CFU/mL in a 96-well plate. 100 uL of phages in modified-LB were aliquoted to the 96-well with bacteria to reach the target MOI in a total volume of 150 µL, topped with 15 µL of mineral oil to prevent evaporation, and covered with a gas-permeable sealing membrane (USA Scientific, Cat. No. 9123-6100). The final co-cultures were then incubated at 37 °C in an automated spectrophotometer (Biotek Synergy 2, Agilent Technologies, USA) for 48 hours, with 5 seconds of shaking before OD600 was read every 20 min. The control was bacteria incubated with modified-LB instead of phages. Each sample was prepared in triplicates. The Suppression Index (SI%) was calculated from formulation below to quantify the relative suppression of bacterial growth between phage-treated and non-treated condition(57).

$$Suppression\ Index\ (\%) = \frac{AUC_{48h}\ non-treated - AUC_{48h}\ phage-treated}{AUC_{48h}\ non-treated}$$

$$AUC = area\ under\ the\ curve$$

Zone of inhibition (ZOI) assay

The subculture of overnight PAO1 culture of OD600 of 0.65 dropped and spreaded onto a Mueller-Hinton agar plate and air-dried. 100 uL of HA-PEG hydrogel (5 mg/mL HA-SH, 1 mg/mL HBPEG, 75 mg/mL of 4-arm PEGs with 10% 4BLD and 90% 4ALD, and 10^{11} PFU/mL PAML-31-1 phage) were pre-formed and transferred to the inoculated agar plate after 3.5 hours of gelation. The hydrogel was allowed to seal with

the agar surface for 15 min, before inverting and incubating at 37 °C for 24 hours. The zone of inhibition (ZOI) was measured.

In vitro biofilm assay and confocal microscopy

The overnight culture of PAO1-GFP was diluted to OD600 of 0.05 in the tryptic soy broth (TSB) and kept on ice. 250 uL of top agar was solidified in each glass bottom 24-well plate (Cellvis, USA, Cat. No. P24-1.5H-N) before adding 300 uL of inoculum. Inoculum was allowed to adhere for 30 min in the incubator at 37ºC, then the media was gently replaced with 500 uL of TSB. After 5 hours, each well was replaced with 800 uL of fresh TSB then incubated overnight. At 24 hours, each well was gently rinsed with 800 uL of PBS+Mg, then replaced with 300 uL of modified-LB, followed by adding treatments. Control treatment was 200 uL of PBS+Mg and phage treatment was 200 uL at 10^{11} PFU/mL adding directly into wells. Empty gel (EG) treatment was 100 uL of HA-PEG gel in Transwell insert topped with 200 uL of PBS+Mg, and HydroPhage (HP) treatment was 100 uL of HA-PEG gel containing PAML-31-1 at 10^{11} PFU/mL in Transwell insert topped with 200 uL of PBS+Mg. Biofilm was monitored with a laser-scanning Leica SP8 confocal microscope with 25x 0.95-NA water immersion objective at 0, 3, 8, and 21 hours. Media was not removed or replaced in between imaging time points to minimize the disturbance of biofilm and hydrogels. Biofilm density was quantified as the percentage of area with PAO1-GFP signal at the base of biofilm, the biofilm and agar interface, and biofilm density change was defined as the change of biofilm density at 21 hours normalized to initial density of each sample. Due to the significant presence of planktonic bacteria in the background above biofilm and/or the significant disruption of biofilm from treatments, the biofilm thickness was manually defined from the biofilm and media boundary to the base of biofilm determined from x-z and y-z projections. 3D rendering of biofilm was reconstructed with Imaris imaging software (Oxford Instruments).

In vitro and *in vivo* bioluminescence to CFU (BLI-CFU) correlation

A dilution series of *Pseudomonas aeruginosa* Xen 41 (PerkinElmer, MA, USA) was prepared in a black 96-well plate (ThermoFisher Scientific, USA, Cat. No. 165305) ranging from 10^0 to 10^7 CFU/well in a total volume of 100 µL. Samples were prepared in triplicate. CFU counts were verified by plating on nonselective LB agar plates. Measurements of luminescent flux were performed as described later in the Methods.

In vitro cytotoxicity and activation of hydrogel against RAW264.7 macrophages

A transwell exposure assay was used to measure the cytotoxicity and immunogenicity of pre-formed hydrogels against RAW264.7 murine macrophage-like cells (**Supplementary Fig. 6a)**. RAW264.7 cells were grown to passage 6 post-thaw in complete DMEM (DMEM/F12 + 10% fetal bovine serum + 1% penicillin/streptomycin). 5 x 10^4 cells were seeded in 24-well tissue culture-treated plates. After overnight incubation, the media was replaced with 500 µL of fresh cDMEM. Cells were treated for 24 h with media only (control), 8% DMSO (positive cytotoxicity control), 1 µg/mL *Escherichia coli* lipopolysaccharide (M1 polarizing positive control; Sigma-Aldrich, Cat. No. L3024-5mg), 20 ng/mL mouse IL-4 (M2 polarizing positive control; ThermoFisher Scientific, USA, Cat. No. 214-14-1MG), FPLC-purified PAML-31-1 at 10^{10} PFU/mL, or 100 µL hydrogels in transwell inserts, with 200 µL of fresh media on top of the hydrogel to prevent drying. After 24 h incubation, media was removed and cells were rinsed once in PBS and stained with 300 µL of 1:3000 IRDye 800CW in PBS for 15 minutes at room temperature. Staining was quenched by the addition of 1 mL ice-cold FACS buffer. After centrifugation, cells were resuspended in 300 µL of anti-mouse CD16/32 (Fc block) in FACS at a concentration of 1 µg/1M cells for 10 min at 4 ºC. After centrifugation and removal of excess Fc block, samples were stained with antibodies (listed below) for 20 min at 4 ºC in a staining volume of 300 µL. Samples were rinsed twice in ice-cold FACS and fixed in 500 µL 10% neutral buffered formalin (ThermoFisher Scientific, USA, Cat. No. 9990245) for 15 minutes at room temperature. Cells were scraped and transferred to a 96-well V-bottom plate for analysis by flow cytometry within 1 week.

Delayed treatment mouse infection model

Male C57BL/6J mice were purchased from the Jackson Laboratory (Jackson Laboratory, #000664). All experiments and animal use procedures were approved by the Institutional Animal Care and Use Committee (IACUC) at the School of Medicine at Stanford University. The study design was adapted from previous work (82). Briefly, 6-7-week-old male mice were anesthetized using 3% isoflurane and shaved. The shaved area was cleaned with povidone-iodine (Dynarex, USA, Cat. No. 1201) and isopropyl alcohol

swabs. Mice received 0.1-0.5 mg/kg slow-release buprenorphine (ZooPharm, USA) subcutaneously as an analgesic. A single circular midline dorsal full-thickness wound was created using a 6 mm biopsy punch (Integra Miltex, Catalog No.12-460-412). The wounds were immediately covered with Tegaderm (3M, USA, Cat. No. 1642W) with silicone adhesive (Vapon, USA, Cat. No. NTL1). Mice were placed in padded plastic collars (Saf-T-Shield, KVP International, USA, Cat. No. RCM) to prevent the removal of wound dressings. Mice received 500 µL of 0.9% normal saline by IP injection on the wounding day and food pellets covered with veterinary nutrient supplements (California Veterinary Supply, USA, Cat. No. HS-10033).

On the infection day, *Pa* Xen41 was grown in LB at 37 ^{o}C with shaking to mid-log phase. Bacteria were pelleted by centrifugation, resuspended in PBS, diluted to 1.25 x 10^7 CFU/mL, and verified by plating on LB agar plates. 24 h post-wounding, wounds were inoculated with 40 µL Xen41 under Tegaderm using an insulin needle at 5 x 10^5 CFU per wound. Bioluminescence images were obtained 1 h post-infection to confirm inoculum was properly injected under the Tegaderm.

24 h post-infection, all mice were imaged ("Day 1") before the first treatment. Mice were treated with 1) PBS control; 2) dorsal penile vein injection (IV), 1 x 10^{11} PFU/mL; 3) high dose one-time topical bolus (HD), 1 x 10^{11} PFU/mL; 4) low dose one-time topical bolus (LD), 2.5 x 10^{10} PFU/mL; 5) daily topical bolus (DD), 2.5 x 10^{10} PFU/mL, for 4 days; or 6) HydroPhage (HP), 1 x 10^{11} PFU/mL. All mice were weighed daily. Additional Tegaderm dressings were applied to existing ones if the dressing became loose. Mice that removed Tegaderm dressings and had a resultant >2 log reduction in luminescent flux were excluded from subsequent analysis. Six days post-infection, mice were euthanized, and the wound was harvested (1 cm^2). Each wound was divided in half. Half of the wound was weighed and homogenized for enumerating colony-forming units (CFU) and plaque-forming units (PFU), and the other half was processed for flow cytometry. The next day, at least 10 colonies from each wound isolate were picked and started an overnight culture, then stored in 30% glycerol at -80 ^{o}C for further characterization, such as planktonic suppression assay.

Bioluminescence imaging (BLI)

Bioluminescence imaging was performed on the Lago X In Vivo Imaging System (Spectral Instruments Imaging, USA). A series of exposures ranging from 5 s to 60 s were taken. The longest exposure without overexposure was used for analysis. The following imaging settings were used: F-stop 1.2, Binning: Heavy, FOV: 25. Images were analyzed using Aura version 4.0 (Spectral Instruments Imaging, USA) by integrating the radiance (photons/s/cm^2/sr) in a region of interest to measure total signal flux (photons/s).

Wound flow cytometry

Wounds were rinsed once in HBSS, blotted to remove excess HBSS, and placed into pre-weighed 1.5 mL polystyrene tubes containing 500 µL ice-cold digestion buffer (RPMI-1640 + 25 mM HEPES, pH 7.4, 1.3 WU/mL Liberase TL (Roche, Switzerland, Cat. No. 05401020001), 2 U/mL bovine DNase I (Roche, Switzerland, Cat. No. 11284932001), 25 mM $MgCl_2$, 1 mM $CaCl_2$, 200 U/mL collagenase IV (Worthington Biochemical, USA. Cat. No. LS004188). Samples were weighed and minced finely using scissors. An additional 500 µL ice-cold digestion buffer was added to samples and incubated at 37 ^{o}C with shaking at 750 x rpm for 2 hours. Samples were inverted several times every 30 minutes during the incubation. After the 2-hour digestion, samples were treated with 100 µL Accutase (Innovative Cell Technologies, San Diego, CA, USA, Cat. No. AT104) and incubated for 20 minutes at room temperature.

Digested samples were passed through a 40 µm nylon cell strainer (Corning, Corning, NY, USA, Cat. No. 352340) pre-wetted with 1 mL of ice-cold FACS buffer (PBS + 1 mM EDTA + 1% BSA). Samples were pressed through the strainer using the rubber end of a syringe plunger. Cell strainers were rinsed with 5 mL of ice-cold FACS buffer. Cells were pelleted by centrifugation (500 x g, 10 min, 4 ^{o}C), and the supernatant was aspirated. Pellets were resuspended in 1 mL ice-cold FACS buffer and pelleted again. Pellets were resuspended in 250 µL of room temperature ACK red blood cell lysis buffer (0.15 M NH_4Cl, 10 mM $KHCO_3$, 0.1 mM EDTA, pH 7.3) and incubated for precisely 4 minutes (variation <5 seconds), after which lysis was stopped by the addition of 750 µL of PBS.

Cells were then pelleted by centrifugation (500 x g, 20 min), removed supernatant, and resuspended in 200 µL ice-cold FACS buffer. 10 µL samples were diluted into a final volume of 200 µL and counted on a flow cytometer. 650,000 cells/sample were aliquoted to a 96-well V-bottom tissue culture-treated plate (Corning,

Corning, USA, Cat. No. 07-200-96). The remaining cells were pooled and aliquoted for unstained, single-stained, and fluorescence-minus-one (FMO) controls.

For staining, cells were rinsed once in ice-cold FACS buffer and then stained in 50 µL 1:3000 IRDye 800CW Live/Dead NIR stain in PBS for 15 minutes at room temperature. Staining was quenched by the addition of 150 µL of ice-cold FACS buffer. After centrifugation, cells were resuspended in 30 µL of anti-mouse CD16/32 (Fc block) in FACS at a concentration of 1 µg/million cells for 10 min at 4 ^{o}C. After centrifugation and removal of excess Fc block, samples were stained with antibodies (listed below) for 20 min at 4 ^{o}C in a staining volume of 30 µL. Samples were then rinsed twice in ice-cold FACS and fixed in 200 uL 4% paraformaldehyde (20 min, room temperature). Samples were then resuspended in 200 µL FACS and acquired on the Cytek Aurora NL-3000 spectral flow cytometer (Cytek Biosciences, CA, USA) within 1 week of fixation. Spectral unmixing was performed using narrow gates and without unmixing autofluorescence.

Statistical analyses

Statistical analyses were performed on GraphPad Prism version 10. Ordinary one-way analysis of variance (ANOVA) with Tukey post-hoc tests were used for multiple comparisons unless noted. Unpaired two-tailed Student's *t*-tests were used for comparison between two groups unless otherwise mentioned. $P < 0.05$ was considered significant unless otherwise noted. Error bars represent the standard deviation (S.D.), unless otherwise noted. * $P \leq 0.05$, ** $P \leq 0.01$, *** $P \leq 0.001$, and **** $P \leq 0.0001$.

Acknowledgements

In vivo imaging was performed at Stanford Center for Innovation in *In Vivo* Imaging (Sci^3). We thank A. Khosravi, A. Saraswathibhatla, D. Indana and other members from Bollyky and Chaudhuri lab for their scientific inputs; the staff at the Sci^3 for providing the support needed to perform the required experiments, including F. Habte. Research reported in this publication was supported by Stanford Catalyst Grant. Q. C. discloses support from Cystic Fibrosis Foundation CHEN21F0, Cystic Fibrosis Research Institute, and Stanford Maternal & Child Health Research Institute. T.D. discloses support from NIH grant T32-GM007365; Stanford Interdisciplinary Graduate Fellowship, Gold Family Graduate Fellow. M.H. discloses support from National Institutes of Health grants R00-EB028838. P.L.B discloses support from National Institutes of Health grant R01 HL148184-01; National Institutes of Health grant R01 AI12492093; National Institutes of Health grant R01 DC019965; Cystic Fibrosis Foundation grant; Emerson Collective grant. The contents are those of the authors and do not necessarily represent the view of the funding agencies.

Competing interests

The authors declare no competing interests

References

1. Høiby N, Ciofu O, Johansen HK, Song Z jun, Moser C, Jensen PØ, et al. The clinical impact of bacterial biofilms. Int J Oral Sci. 2011 Apr;3(2):55–65.
2. Bryers JD. Medical biofilms. Biotechnol Bioeng. 2008 May 1;100(1):1–18.
3. Sen CK, Gordillo GM, Roy S, Kirsner R, Lambert L, Hunt TK, et al. Human skin wounds: a major and snowballing threat to public health and the economy. Wound Repair Regen. 2009;17(6):763–71.
4. Lister PD, Wolter DJ, Hanson ND. Antibacterial-Resistant *Pseudomonas aeruginosa* : Clinical Impact and Complex Regulation of Chromosomally Encoded Resistance Mechanisms. Clin Microbiol Rev. 2009 Oct;22(4):582–610.
5. Kapel N, Caballero JD, MacLean RC. Localized pmrB hypermutation drives the evolution of colistin heteroresistance. Cell Rep. 2022 Jun;39(10):110929.
6. Olalekan A, Bader BK, Iwalokun B, Wolf S, Lalremruata A, Dike A, et al. High incidence of carbapenemase-producing *Pseudomonas aeruginosa* clinical isolates from Lagos, Nigeria. JAC Antimicrob Resist. 2023 Mar 2;5(2).
7. Ogbolu DO, Piddock LJV, Webber MA. Opening Pandora's box: High-level resistance to antibiotics of last resort in Gram-negative bacteria from Nigeria. J Glob Antimicrob Resist. 2020 Jun;21:211–7.
8. Woodford N, Palepou MFI, Babini G, Bates J, Livermore D. Carbapenemase-producing Pseudomonas aeruginosa in UK. The Lancet. 1998 Aug;352(9127):546–7.
9. Butler MS, Gigante V, Sati H, Paulin S, Al-Sulaiman L, Rex JH, et al. Analysis of the Clinical Pipeline of Treatments for Drug-Resistant Bacterial Infections: Despite Progress, More Action Is Needed. Antimicrob Agents Chemother. 2022 Mar 15;66(3).
10. Reig S, Le Gouellec A, Bleves S. What Is New in the Anti–Pseudomonas aeruginosa Clinical Development Pipeline Since the 2017 WHO Alert? Front Cell Infect Microbiol. 2022 Jul 8;12.
11. Kirketerp-Møller K, Jensen PØ, Fazli M, Madsen KG, Pedersen J, Moser C, et al. Distribution, organization, and ecology of bacteria in chronic wounds. J Clin Microbiol. 2008 Aug;46(8):2717–22.
12. Dowd SE, Sun Y, Secor PR, Rhoads DD, Wolcott BM, James GA, et al. Survey of bacterial diversity in chronic wounds using Pyrosequencing, DGGE, and full ribosome shotgun sequencing. BMC Microbiol. 2008;8(1):43.
13. Malic S, Hill KE, Hayes A, Percival SL, Thomas DW, Williams DW. Detection and identification of specific bacteria in wound biofilms using peptide nucleic acid fluorescent in situ hybridization (PNA FISH). Microbiology (N Y). 2009 Aug 1;155(8):2603–11.
14. James GA, Swogger E, Wolcott R, Pulcini E deLancey, Secor P, Sestrich J, et al. Biofilms in chronic wounds. Wound Repair and Regeneration. 2008 Jan 13;16(1):37–44.
15. Lipsky BA, Berendt AR, Deery HG, Embil JM, Joseph WS, Karchmer AW, et al. Diagnosis and Treatment of Diabetic Foot Infections. Clinical Infectious Diseases. 2004 Oct 1;39(7):885–910.
16. Centers for Disease Control and Prevention. National Diabetes Statistics Report website.
17. Chen Q, Dharmaraj T, Cai PC, Burgener EB, Haddock NL, Spakowitz AJ, et al. Bacteriophage and Bacterial Susceptibility, Resistance, and Tolerance to Antibiotics. Pharmaceutics [Internet]. 2022/07/28. 2022;14(7). Available from: https://www.ncbi.nlm.nih.gov/pubmed/35890320
18. d'Herelle F. An Addresson BACTERIOPHAGY AND RECOVERY FROM INFECTIOUS DISEASES. Can Med Assoc J. 1931 May;24(5):619–28.
19. Wittebole X, De Roock S, Opal SM. A historical overview of bacteriophage therapy as an alternative to antibiotics for the treatment of bacterial pathogens. Virulence. 2014 Jan 1;5(1):226–35.
20. Fiedler AW, Gundersen MS, Vo TP, Almaas E, Vadstein O, Bakke I. Phage therapy minimally affects the water microbiota in an Atlantic salmon (Salmo salar) rearing system while still preventing infection. Sci Rep [Internet]. 2023;13(1):1–13. Available from: https://doi.org/10.1038/s41598-023-44987-7
21. Kovacs CJ, Rapp EM, McKenzie SM, Mazur MZ, Mchale RP, Brasko B, et al. Disruption of Biofilm by Bacteriophages in Clinically Relevant Settings. Mil Med. 2023;00.
22. Burrowes B, Harper DR, Anderson J, McConville M, Enright MC. Bacteriophage therapy: potential uses in the control of antibiotic-resistant pathogens. Expert Rev Anti Infect Ther. 2011 Sep;9(9):775–85.

23. Maddocks S, Fabijan AP, Ho J, Lin RCY, Ben Zakour NL, Dugan C, et al. Bacteriophage Therapy of Ventilator-associated Pneumonia and Empyema Caused by Pseudomonas aeruginosa. Am J Respir Crit Care Med. 2019 Nov 1;200(9):1179–81.
24. Cano EJ, Caflisch KM, Bollyky PL, Van Belleghem JD, Patel R, Fackler J, et al. Phage Therapy for Limb-threatening Prosthetic Knee Klebsiella pneumoniae Infection: Case Report and In Vitro Characterization of Anti-biofilm Activity. Clin Infect Dis [Internet]. 2020/07/24. 2021;73(1):e144–51. Available from: https://www.ncbi.nlm.nih.gov/pubmed/32699879
25. Chan BK, Turner PE, Kim S, Mojibian HR, Elefteriades JA, Narayan D. Phage treatment of an aortic graft infected with *Pseudomonas aeruginosa*. Evol Med Public Health. 2018 Jan 1;2018(1):60–6.
26. Echterhof A, Dharmaraj T, McBride R, Berry J, Hopkins M, Selvakumar H, et al. The contribution of neutrophils to bacteriophage clearance and pharmacokinetics in vivo. bioRxiv. 2024 Jan 27;
27. Le T, Nang SC, Zhao J, Yu HH, Li J, Gill JJ, et al. Therapeutic Potential of Intravenous Phage as Standalone Therapy for Recurrent Drug-Resistant Urinary Tract Infections. Antimicrob Agents Chemother. 2023 Apr 18;67(4):e0003723.
28. Abedon ST, Kuhl SJ, Blasdel BG, Kutter EM. Phage treatment of human infections. Bacteriophage. 2011 Mar 22;1(2):66–85.
29. Kutter E, De Vos D, Gvasalia G, Alavidze Z, Gogokhia L, Kuhl S, et al. Phage Therapy in Clinical Practice: Treatment of Human Infections. Curr Pharm Biotechnol. 2010 Jan 1;11(1):69–86.
30. Karinja SJ, Spector JA. Treatment of Infected Wounds in the Age of Antimicrobial Resistance: Contemporary Alternative Therapeutic Options. Plast Reconstr Surg. 2018 Oct;142(4):1082–92.
31. Duplessis CA, Biswas B. A Review of Topical Phage Therapy for Chronically Infected Wounds and Preparations for a Randomized Adaptive Clinical Trial Evaluating Topical Phage Therapy in Chronically Infected Diabetic Foot Ulcers. Antibiotics (Basel). 2020 Jul 4;9(7).
32. Morozova V V, Kozlova YN, Ganichev DA, Tikunova N V. Bacteriophage Treatment of Infected Diabetic Foot Ulcers. Methods Mol Biol. 2018;1693:151–8.
33. Steele A, Stacey HJ, de Soir S, Jones JD. The Safety and Efficacy of Phage Therapy for Superficial Bacterial Infections: A Systematic Review. Antibiotics (Basel). 2020 Oct 29;9(11).
34. Chang RYK, Morales S, Okamoto Y, Chan HK. Topical application of bacteriophages for treatment of wound infections. Transl Res. 2020 Jun;220:153–66.
35. Vonasek E, Lu P, Hsieh YL, Nitin N. Bacteriophages immobilized on electrospun cellulose microfibers by non-specific adsorption, protein–ligand binding, and electrostatic interactions. Cellulose. 2017 Oct 10;24(10):4581–9.
36. Shafigh Kheljan F, Sheikhzadeh Hesari F, Aminifazl MS, Skurnik M, Gholadze S, Zarrini G. Design of Phage-Cocktail–Containing Hydrogel for the Treatment of Pseudomonas aeruginosa–Infected Wounds. Viruses. 2023 Mar 21;15(3):803.
37. Kim HY, Chang RYK, Morales S, Chan HK. Bacteriophage-Delivering Hydrogels: Current Progress in Combating Antibiotic Resistant Bacterial Infection. Antibiotics. 2021 Jan 29;10(2):130.
38. Patpatia S, Schaedig E, Dirks A, Paasonen L, Skurnik M, Kiljunen S. Rapid hydrogel-based phage susceptibility test for pathogenic bacteria. Front Cell Infect Microbiol. 2022;12:1032052.
39. Ma Y, Pacan JC, Wang Q, Xu Y, Huang X, Korenevsky A, et al. Microencapsulation of bacteriophage felix O1 into chitosan-alginate microspheres for oral delivery. Appl Environ Microbiol. 2008 Aug;74(15):4799–805.
40. Barros JAR, Melo LDR de, Silva RAR da, Ferraz MP, Azeredo JCV de R, Pinheiro VM de C, et al. Encapsulated bacteriophages in alginate-nanohydroxyapatite hydrogel as a novel delivery system to prevent orthopedic implant-associated infections. Nanomedicine. 2020 Feb;24:102145.
41. Korehei R, Kadla JF. Encapsulation of T4 bacteriophage in electrospun poly(ethylene oxide)/cellulose diacetate fibers. Carbohydr Polym. 2014 Jan 16;100:150–7.
42. Rubalskii E, Ruemke S, Salmoukas C, Aleshkin A, Bochkareva S, Modin E, et al. Fibrin glue as a local drug-delivery system for bacteriophage PA5. Sci Rep. 2019 Feb 14;9(1):2091.
43. Markoishvili K, Tsitlanadze G, Katsarava R, Glenn J, Morris Jr. MD, Sulakvelidze A. A novel sustained-release matrix based on biodegradable poly(ester amide)s and impregnated with bacteriophages and an antibiotic shows promise in management of infected venous stasis ulcers and other poorly healing wounds. Int J Dermatol. 2002 Jul 16;41(7):453–8.
44. Wroe JA, Johnson CT, García AJ. Bacteriophage delivering hydrogels reduce biofilm formation in vitro and infection in vivo. J Biomed Mater Res A. 2020 Jan 5;108(1):39–49.

45. Microbeads C modified GH. Alginate- and Chitosan-Modified Gelatin Hydrogel Microbeads for Delivery of E. coli Phages. 2024;
46. Barros JAR, Melo LDR de, Silva RAR da, Ferraz MP, Azeredo JCV de R, Pinheiro VM de C, et al. Encapsulated bacteriophages in alginate-nanohydroxyapatite hydrogel as a novel delivery system to prevent orthopedic implant-associated infections. Nanomedicine. 2020 Feb 1;24.
47. Agarwal R, Johnson CT, Imhoff BR, Donlan RM, McCarty NA, García AJ. Inhaled bacteriophage-loaded polymeric microparticles ameliorate acute lung infections. Nat Biomed Eng [Internet]. 2018;2(11):841–9. Available from: http://dx.doi.org/10.1038/s41551-018-0263-5
48. Wang R, Yeh YJ, An YN, Virly. Engineering pH-sensitive erodible chitosan hydrogel composite containing bacteriophage: An interplay between hydrogel and bacteriophage against Staphylococcus aureus. Int J Biol Macromol [Internet]. 2023;253(P7):127371. Available from: https://doi.org/10.1016/j.ijbiomac.2023.127371
49. Shen HY, Liu ZH, Hong JS, Wu MS, Shiue SJ, Lin HY. Controlled-release of free bacteriophage nanoparticles from 3D-plotted hydrogel fibrous structure as potential antibacterial wound dressing. Journal of Controlled Release [Internet]. 2021;331(October 2020):154–63. Available from: https://doi.org/10.1016/j.jconrel.2021.01.024
50. Barros JAR, Melo LDR de, Silva RAR da, Ferraz MP, Azeredo JCV de R, Pinheiro VM de C, et al. Encapsulated bacteriophages in alginate-nanohydroxyapatite hydrogel as a novel delivery system to prevent orthopedic implant-associated infections. Nanomedicine. 2020 Feb 1;24.
51. Moghtader F, Solakoglu S, Piskin E. Alginate- and Chitosan-Modified Gelatin Hydrogel Microbeads for Delivery of E. coli Phages. Gels. 2024;10(4):244.
52. Kopač T, Lisac A, Mravljak R, Ručigaj A, Krajnc M, Podgornik A. Bacteriophage delivery systems based on composite polyhipe/nanocellulose hydrogel particles. Polymers (Basel). 2021;13(16).
53. Barros JAR, Melo LDR de, Silva RAR da, Ferraz MP, Azeredo JCV de R, Pinheiro VM de C, et al. Encapsulated bacteriophages in alginate-nanohydroxyapatite hydrogel as a novel delivery system to prevent orthopedic implant-associated infections. Nanomedicine. 2020 Feb 1;24.
54. Agarwal R, Johnson CT, Imhoff BR, Donlan RM, McCarty NA, García AJ. Inhaled bacteriophage-loaded polymeric microparticles ameliorate acute lung infections. Nat Biomed Eng [Internet]. 2018;2(11):841–9. Available from: http://dx.doi.org/10.1038/s41551-018-0263-5
55. Kopač T, Lisac A, Mravljak R, Ručigaj A, Krajnc M, Podgornik A. Bacteriophage delivery systems based on composite polyhipe/nanocellulose hydrogel particles. Polymers (Basel). 2021;13(16).
56. Chang RYK, Okamoto Y, Morales S, Kutter E, Chan HK. Hydrogel formulations containing non-ionic polymers for topical delivery of bacteriophages. Int J Pharm [Internet]. 2021;605(June):120850. Available from: https://doi.org/10.1016/j.ijpharm.2021.120850
57. Burgener EB, Bollyky PL. The Rational Design of Broadly Effective Phage Therapy Cocktails Against Bacterial Infections.
58. Górski A, Międzybrodzki R, Borysowski J, editors. Phage Therapy: A Practical Approach. Cham: Springer International Publishing; 2019.
59. Berkson JD, Wate CE, Allen GB, Schubert AM, Dunbar KE, Coryell MP, et al. Phage-specific immunity impairs efficacy of bacteriophage targeting Vancomycin Resistant Enterococcus in a murine model. Nat Commun. 2024;15(1):1–14.
60. Chegini Z, Khoshbayan A, Taati Moghadam M, Farahani I, Jazireian P, Shariati A. Bacteriophage therapy against Pseudomonas aeruginosa biofilms: A review. Ann Clin Microbiol Antimicrob [Internet]. 2020;19(1):1–17. Available from: https://doi.org/10.1186/s12941-020-00389-5
61. Costerton JW, Stewart PS, Greenberg EP. Bacterial biofilms: a common cause of persistent infections. Science (1979) [Internet]. 1999/05/21. 1999;284(5418):1318–22. Available from: https://www.ncbi.nlm.nih.gov/pubmed/10334980
62. Vlamakis H, Chai Y, Beauregard P, Losick R, Kolter R. Sticking together: building a biofilm the Bacillus subtilis way. Nat Rev Microbiol [Internet]. 2013/01/29. 2013;11(3):157–68. Available from: https://www.ncbi.nlm.nih.gov/pubmed/23353768
63. Mann EE, Wozniak DJ. Pseudomonas biofilm matrix composition and niche biology. FEMS Microbiol Rev [Internet]. 2012/01/04. 2012;36(4):893–916. Available from: https://www.ncbi.nlm.nih.gov/pubmed/22212072
64. Parsek MR, Singh PK. Bacterial biofilms: an emerging link to disease pathogenesis. Annu Rev Microbiol [Internet]. 2003/10/07. 2003;57:677–701. Available from: https://www.ncbi.nlm.nih.gov/pubmed/14527295

65. Dreifke MB, Jayasuriya AA, Jayasuriya AC. Current wound healing procedures and potential care. Mater Sci Eng C Mater Biol Appl. 2015 Mar;48:651–62.
66. Stevens DL, Bisno AL, Chambers HF, Dellinger EP, Goldstein EJC, Gorbach SL, et al. Practice guidelines for the diagnosis and management of skin and soft tissue infections: 2014 update by the infectious diseases society of America. Clinical Infectious Diseases. 2014;59(2).
67. Clinton A, Carter T. Chronic wound biofilms: Pathogenesis and potential therapies. Lab Medicine. 2015;46(4):277–84.
68. Hu J, Chen S, Yang Y, Li L, Cheng X, Cheng Y, et al. A Smart Hydrogel with Anti-Biofilm and Anti-Virulence Activities to Treat Pseudomonas aeruginosa Infections. Adv Healthc Mater. 2022 Jul;11(13):e2200299.
69. Lou J, Stowers R, Nam S, Xia Y, Chaudhuri O. Stress relaxing hyaluronic acid-collagen hydrogels promote cell spreading, fiber remodeling, and focal adhesion formation in 3D cell culture. Biomaterials [Internet]. 2018;154:213–22. Available from: https://doi.org/10.1016/j.biomaterials.2017.11.004
70. Hunt DR, Klett KC, Mascharak S, Wang H, Gong D, Lou J, et al. Engineered Matrices Enable the Culture of Human Patient-Derived Intestinal Organoids. Advanced Science. 2021;8(10):1–12.
71. Ren H, Zhang Z, Cheng X, Zou Z, Chen X, He C. Injectable, self-healing hydrogel adhesives with firm tissue adhesion and on-demand biodegradation for sutureless wound closure. Sci Adv. 2023;9(33):eadh4327.
72. Roth JG, Huang MS, Navarro RS, Akram JT, LeSavage BL, Heilshorn SC. Tunable hydrogel viscoelasticity modulates human neural maturation. Sci Adv. 2023;9(42):eadh8313.
73. Sharma PK, Singh Y. Glyoxylic Hydrazone Linkage-Based PEG Hydrogels for Covalent Entrapment and Controlled Delivery of Doxorubicin. Biomacromolecules. 2019;20(6):2174–84.
74. Hua Y, Gan Y, Li P, Song L, Shi C, Bao C, et al. Moldable and Removable Wound Dressing Based on Dynamic Covalent Cross-Linking of Thiol-Aldehyde Addition. ACS Biomater Sci Eng. 2019 Aug 12;5(8):4048–53.
75. Hua Y, Gan Y, Zhang Y, Ouyang B, Tu B, Zhang C, et al. Adaptable to Mechanically Stable Hydrogels Based on the Dynamic Covalent Cross-Linking of Thiol-Aldehyde Addition. ACS Macro Lett. 2019 Mar 19;8(3):310–4.
76. Dąbrowska K, Miernikiewicz P, Piotrowicz A, Hodyra K, Owczarek B, Lecion D, et al. Immunogenicity studies of proteins forming the T4 phage head surface. J Virol. 2014 Nov;88(21):12551–7.
77. Cavalcante-Silva J, Koh TJ. Role of NK Cells in Skin Wound Healing of Mice. J Immunol. 2023 Apr 1;210(7):981–90.
78. Liippo J, Toriseva M, Kähäri VM. Natural killer cells in wound healing. In: Natural Killer Cells. Elsevier; 2010. p. 519–25.
79. Clark RAF. Overview and General Considerations of Wound Repair. In: The Molecular and Cellular Biology of Wound Repair. Boston, MA: Springer US; 1998. p. 3–33.
80. Sweere JM, Ishak H, Sunkari V, Bach MS, Manasherob R, Yadava K, et al. The Immune Response to Chronic Pseudomonas aeruginosa Wound Infection in Immunocompetent Mice. Adv Wound Care (New Rochelle). 2020 Feb 1;9(2):35–47.
81. Dharmaraj T, Kratochvil MJ, Pourtois JD, Chen Q, Hajfathalian M, Hargil A, et al. Rapid assessment of changes in phage bioactivity using dynamic light scattering. PNAS Nexus. 2023 Dec 1;2(12).
82. Chen JS, Longaker MT, Gurtner GC. Murine models of human wound healing. Methods Mol Biol. 2013;1037:265–74.